Advanced Journal of Chemistry-Section A

Journal homepage: www.ajchem-a.com

Original Research Article

Theoretical Investigations on Thiadiazole Derivatives as Corrosion Inhibitors on Mild Steel

Thomas Aondofa Nyijime [1] *, **Habibat Faith Chahul** [1], **Abdullahi Muhammad Ayuba** [2], **Fater Iorhuna** [2]

[1] *Department of Chemistry, College of Physical Sciences, Federal University of Agriculture, Makurdi, Nigeria*
[2] *Department of Pure and Industrial Chemistry, Faculty of Physical Sciences, Bayero University, Kano, Nigeria*

ARTICLE INFO

Article history

Submitted: 28 January 2023
Revised: 02 March 2023
Accepted: 04 March 2023
Available online: 08 March 2023
Manuscript ID: AJCA-2301-1352
Checked for Plagiarism: Yes

DOI: **10.22034/AJCA.2023.383496.1352**

KEYWORDS

Thiadiazole
Iron
Adsorption
Corrosion
Fukui indices

ABSTRACT

Experimental methods have been employed to elucidate the corrosion inhibition mechanism, but they are often expensive and time-consuming, necessitating the search for more alternatives. The development of computer hardware and software engineering has allowed the effective use of theoretical modeling tools that successfully correlate the inhibition efficiency of the inhibitors with their molecular structure and properties. In this study, computational methods were used to further explain the mode and mechanism of the thiadiazoles inhibition on Fe surface whose studies were reported in the literature as Thiadiazoles-A potential class of heterocyclic inhibitors for prevention of mild steel corrosion in hydrochloric acid solution. Parameters including quantum chemical through DFT and molecular dynamic simulations of studied molecules on Fe surfaces were performed. Results obtained by calculating these thiadiazoles' adsorption or binding energies were in good agreement with the experimentally reported results elsewhere. Concerning the calculated adsorption or binding energies, their relatively low values inferred that the compounds are weakly adsorbed onto the surface of Fe through Van der Waals forces and therefore obey the mechanism of physical adsorption. Fukui indices values revealed that the active sites were found to be located on the molecules heteroatoms (Sulphur and Nitrogen). It was also established that the reference molecule thiadiazole (TDA) was the least adsorbed when compared to the other four molecules of its derivatives. The order of the inhibition efficiency as determined is as follows: PAT > EAT > MAT > AT > TDA

GRAPHICAL ABSTRACT

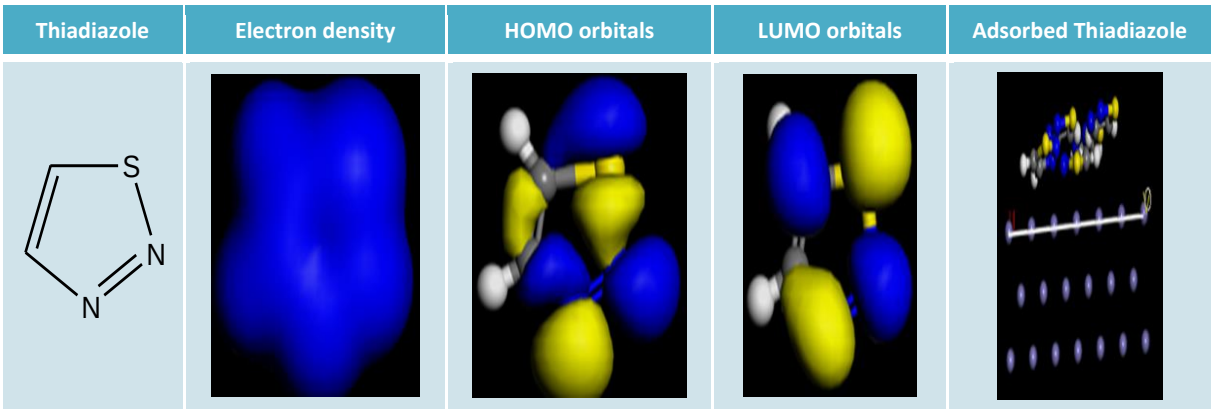

* Corresponding author: Nyijime, Thomas Aondofa
✉ E-mail: nyijime.thomas@uam.edu.ng

Introduction

In concrete reinforcement, iron is often utilized as building materials in the form of iron bars and machinery components, among other substances. It is essential to numerous industries. Unfortunately, iron corrosion generates significant problems for civilization [1-6]. It is well known that organic compounds can be used as inhibitors in the form of recognized substances or plant extracts in industrial settings to delay the corrosive process of steel against metal surfaces [6-8]. To prevent iron from corroding in acidic solutions, heterocyclic compounds with lone pairs of electrons in their heteroatoms-such as sulfur, nitrogen, and oxygen delocalized electrons in their molecules, are used [3-13]. Experimental methods are essential for explaining the inhibition process, but they are often expensive and time-consuming. The ongoing advancement of hardware and software has opened the door for the effective application of theoretical chemistry in corrosion inhibition research [14–16]. The derivatives of thiadiazoles are heterocyclic compounds and have been widely reported in the literature [3, 16-19]. Compounds containing nitrogen and sulfur atoms are particularly important as they often provide excellent inhibition compared to those containing only nitrogen or sulphur [10-14]. Owing to their extensive lone pair, π-conjugation and the presence of heteroatoms, their use as corrosion inhibitors could be well explored as the need to continuously search for more anti-corrosive agents remains very important [3-6]. Theoretical correlations between molecular, electronic, and structural features and such compounds experimentally verified corrosion inhibition efficiencies are typically made using molecular dynamics and quantum chemistry techniques [20,21]. The derivatives of thiadiazole molecules are an example of such compounds [19].

In this current study, the established phytochemicals from the thiadiazole compound and some of its derivatives were employed to examine whether their ability can prevent the corrosion of iron metal surfaces. Computationally, this work is accomplished by computing and simulating quantum chemical parameters using molecular dynamics. The structures of the investigated compounds are demonstrated in Figure 1. Whose study was reported experimentally by Quraishi and Khan [19].

Computational Method

The Materials Studio 7.0 program (Accelrys, Inc.) DMOL3 package was utilized to thoroughly optimize and calculate the molecular properties of the investigated inhibitor molecules. Based on density functional theory, quantum chemical parameters were conducted utilizing the B3LYP functional and DNP basis set in the aqueous phase (DFT). Molecular area, electronegativity (χ), hardness (η), and softness (σ), energy gaps ((ΔE), the energy of the lowest unoccupied molecular orbitals (E_{LUMO}), the energy of the highest molecular orbitals (E_{HOMO}), and molecular area $\left(\overset{0}{A}2\right)$, Molecular volume ($\overset{0}{A}3$) Energy of back donation electron, Nucleophilicity, and global electrophilicity index (ω), Nucleophilicity (ε), Energy of back donation electron ($\Delta E_{b\text{-}d}$) and local reactivity, such as the Fukui function f(r) and percentage of second-order Fukui derivatives, were evaluated based on the DFT principle. These variables would further provide more information about these compound's chemical reactivity and selectivity [2,14], [16–19].

The chemical potential (μ) is equal to the negative value of the electronegativity (x) if the potential energy ($\vec{r}$) and total energy (E) of electrons are fixed. Equation (1) illustrates the relationship between μ and x in terms of the first

derivatives of E with the N atom at constant v(r) [20].

$$\mu = -x = \left(\frac{\partial E}{\partial N}\right)(\vec{r}) \quad (1)$$

According to eq. (2) [21], "hardness" in DFT is defined as the second derivative of the system's total energy to its total number of electrons:

$$\eta = \left(\frac{\partial \mu}{\partial \mu}\right)(\vec{r}) = \frac{1}{2}\left(\frac{\partial^2 E}{\partial N^2}\right)v(\vec{r}) \quad (2)$$

The reciprocal of the absolute hardness is the global softness (σ), written as:

$$\sigma = \frac{1}{\eta} = \left(\frac{\partial N}{\partial \mu}\right)(\vec{r}) \quad (3)$$

Equations 4 and 5 show a direct relationship between ionization potential (I) and electron affinity (EA) and the energies of the highest occupied molecular orbital (E_{HOMO}) and the lowest unoccupied molecular orbital (E_{LUMO}), respectively [22-23]:

$$IP = -E_{HOMO} \quad (4)$$

$$EA = -E_{LUMO} \quad (5)$$

The equations below indicate some of the values associated with ionization potential (IP) and electron affinity (EA):

$$\Delta E = E_{HOMO} - E_{LUMO} \quad (6)$$

$$x = \frac{(IP + EA)}{2} \quad (7)$$

$$\eta = \frac{(IP - EA)}{2} \quad (8)$$

$$\omega = \frac{\mu^2}{2\eta} = \frac{\chi^2}{2\eta} \quad (9)$$

$$\varepsilon = \frac{1}{\omega} \quad (10)$$

$$\Delta E_{b-d} = -\frac{\eta}{4} = \frac{1}{8}(E_{HOMO} - E_{LUMO}) \quad (11)$$

Using equation (12) and the determined values for x and η, the percentage of electrons transported from the inhibitor molecule to the Fe metal surface was estimated as follows.

$$\Delta N = \frac{(\chi Fe - \chi inh)}{2(\eta Fe + \eta inh)} \quad (12)$$

Whereas χ_{Fe} and χ_{inh} stand for the absolute hardness of Fe and the inhibitor molecule, respectively, and η_{Fe} and η_{inh} describe the absolute electronegativity of Fe metal, respectively. Theoretical parameters included the bulk iron electronegativity of χ_{Fe}=7 eV and its global hardness of 0 [24]. Using Fukui indices, the active site of thiadiazole and its derivatives were assessed. According to equation (13) [25-27], the Fukui index ($\vec{r}$) is the first-order partial derivative of the electron density ($\vec{r}$) to the electron number N.

$$(\vec{r}) = \frac{\partial \rho(\vec{r})\rho(\vec{r})}{\partial N} \quad (13)$$

With the condition of finite-difference approximation, the Fukui index ($\vec{r}$) can be expressed as

$$F(\vec{r})^+ = qi\,(N+1) - qi\,(N) \text{ (for nucleophilic attack)} \quad (14)$$

$$F(\vec{r})^- = qi\,(N) - qi\,(N-1) \text{ (for nucleophilic attack)} \quad (15)$$

Where, $qi\,(N)$, $qi\,(N+1)$, $qi\,(N-1)$ are defined as the atomic charges of the neutral, cationic, and anionic species respectively. $(\vec{r})^+$ and $(\vec{r})^-$ represent the nucleophilic attacking index and the electrophilic attacking index, respectively. The derivative of the second-order Fukui function is defined by the distinction between nucleophilic and electrophilic reactions (f^2). Site k favors a nucleophilic assault if $f^2(r) > 0$, whereas site k prefers an electrophilic attack if $f^2(r)$ 0. This suggests that $f^2(r)$ is a selectivity indicator for nucleophilic or electrophilic assaults.

$$f(r) = f^+ - f^- = f^2 \quad \text{(Fukui function)} \quad (16)$$

On the other hand, the forcite quench tool included in the BOVIA materials studio program was used to do molecular dynamic simulations. The most stable and densely packed atom surface, Fe (110), was used to imitate each inhibitor molecule. A COMPASS force field and Smart algorithm were used in a simulation box measuring 17 by 12 by 28 with a periodic boundary condition to simulate a representative portion of the surface. By creating a 5 x 5 supercell, the iron crystal was split along the (110) plane with a fractional depth of 3.0, and its periodicity was altered. Building TDA molecules and perfecting their geometries came next. The system will be developed via layer builder to arrange the TDA molecules on the Fe (110) surface once the surface, TDA, and its molecules have been minimized. The behaviors of the TDA molecules on the Fe (110) surface were simulated using the COMPASS force field. The MD simulation was run at 298 K in an NVT ensemble for 50 ps of simulation duration and 0.1 fs of the time step. The following equation [2, 15, 28] was used to compute the interaction energy between the inhibitor molecule and the Fe (110) surface:

$$E_{Adsorption} = E_{total} - (E_{inhibitor} + E_{Fe\ surface}) \quad (17)$$

When $E_{Adsorption}$ is the energy of adsorption, E_{total} is the energy of the molecule plus the Fe (110) surface, $E_{inhibitor}$ is the energy of the inhibitor molecule alone, and E_{Fe} surface is the energy of the Fe (110) surface alone.

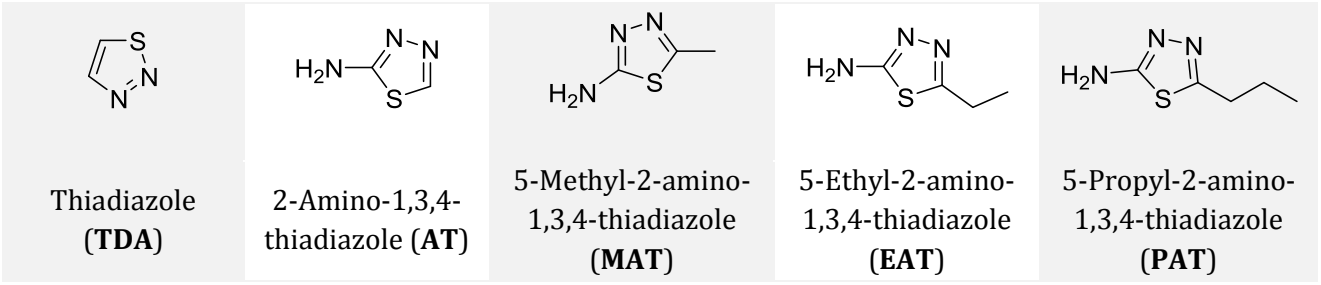

Thiadiazole (**TDA**) | 2-Amino-1,3,4-thiadiazole (**AT**) | 5-Methyl-2-amino-1,3,4-thiadiazole (**MAT**) | 5-Ethyl-2-amino-1,3,4-thiadiazole (**EAT**) | 5-Propyl-2-amino-1,3,4-thiadiazole (**PAT**)

Figure 1. Structures of studied thiadiazoles

Results and Discussion

Molecular Geometry

At the DFT level of theory, the thiadiazole and its derivatives geometries were fully optimized using a B3LYP functional and DNP basis set in the aqueous phase. The bond lengths and angles of the compounds under study are shown in Table 1.

It can be seen from (Table 1) that the single bond S_1-C_2 bond length in the thiadiazole ring of all the molecules are longer and larger than the single bond in C_8-C_9 bond length in PAT (1.527 nm), the single bond C_7-C_8 bond length in EAT and PAT (1.524 and 1.526 nm), and the single bond in C_5-C_7 bond length in MAT, EAT, and PAT (1.487, 1.496 and 1.497 nm) respectively. The double bond in N_3-N_4 bond length in both molecules (1.375 nm) are longer than the N_4-C_5 double bond in the four studied molecule (1.293 nm) and larger in the reference molecule (TDA) (1.371 nm) compared to the four others.

From (Table 1) it can be seen that the bond angles of the four studied molecules together with the reference mole TDA are in the range of 110.543 to 126.743^0.

Table 1. Optimized geometric parameters of thiadiazole (TDA, the reference molecule) and similar structure of 2-amino-1,3,4-thiadiazole (AT), 5-methyl-2-amino-1,3,4-thiadiazole (MAT), 5-ethyl-2-amino-1,3,4-thiadiazole (EAT) and 5-propyl-2-amino-1,3,4-thiadiazole (PAT) molecules

TDA		**AT**		**MAT**	
Bond length	**(nm)**	**Bond length**	**(nm)**	**Bond length**	**(nm)**
S_1-N_2	1.705	S_1-C_2	1.761	S_1-C_2	1.753
N_2-N_3	1.283	C_2-N_3	1.312	C_2-C_6	1.360
N_3-N_4	1.350	C_2-N_6	1.342	C_2-N_3	1.306
N_4-C_5	1.371	N_3-N_4	1.369	N_3-N_4	1.372
		N_4-C_5	1.289	N_4-C_5	1.293
				C_5-C_7	1.487
Bond angle	**(⁰)**	**Bond angle**	**(⁰)**	**Bond angle**	**(⁰)**
S_1-N_2-N_3	110.543	S_1-C_2-N_3	113.205	S_1-C_2-N_3	113.366
N_2-N_3-N_4	114.966	S_1-C_2-N_6	122.177	S_1-C_2-N_6	122.112
N_3-N_4-C_5	113.777	C_2-N_3-N_4	113.013	N_3-N_4-C_5	114.448
		N_3-N_4-C_5	113.194	N_4-C_5-C_7	126.311
				C_5-C_7-C_8	114.169
				C_7-C_8-C_9	112.254
EAT		**PAT**			
Bond length	**(nm)**	**Bond length**	**(nm)**		
S_1-C_2	1.755	S_1-C_2	1.757		
C_2-N_6	1.360	C_2-N_6	1.361		
C_2-N_3	1.305	C_2-N_3	1.305		
N_3-N_4	1.375	N_3-N_4	1.373		
N_4-C_5	1.290	N_4-C_5	1.291		
C_5-C_7	1.496	C_5-C_7	1.497		
C_7-C_8	1.524	C_7-C_8	1.526		
		C_8-C_9	1.527		
Bond angle	**(⁰)**	**Bond angle**	**(⁰)**		
S_1-C_2-N_3	113.474	S_1-C_2-N_6	122.112		
S_1-C_2-N_6	121.695	S_1-C_2-N_6	122.112		
N_3-N_4-C_5	114.414	N_3-N_4-C_5	114.448		
N_4-C_5-C_7	126.743	N_4-C_5-C_7	126.311		
C_5-C_7-N_6	121.695	C_7-C_8-C_9	112.254		

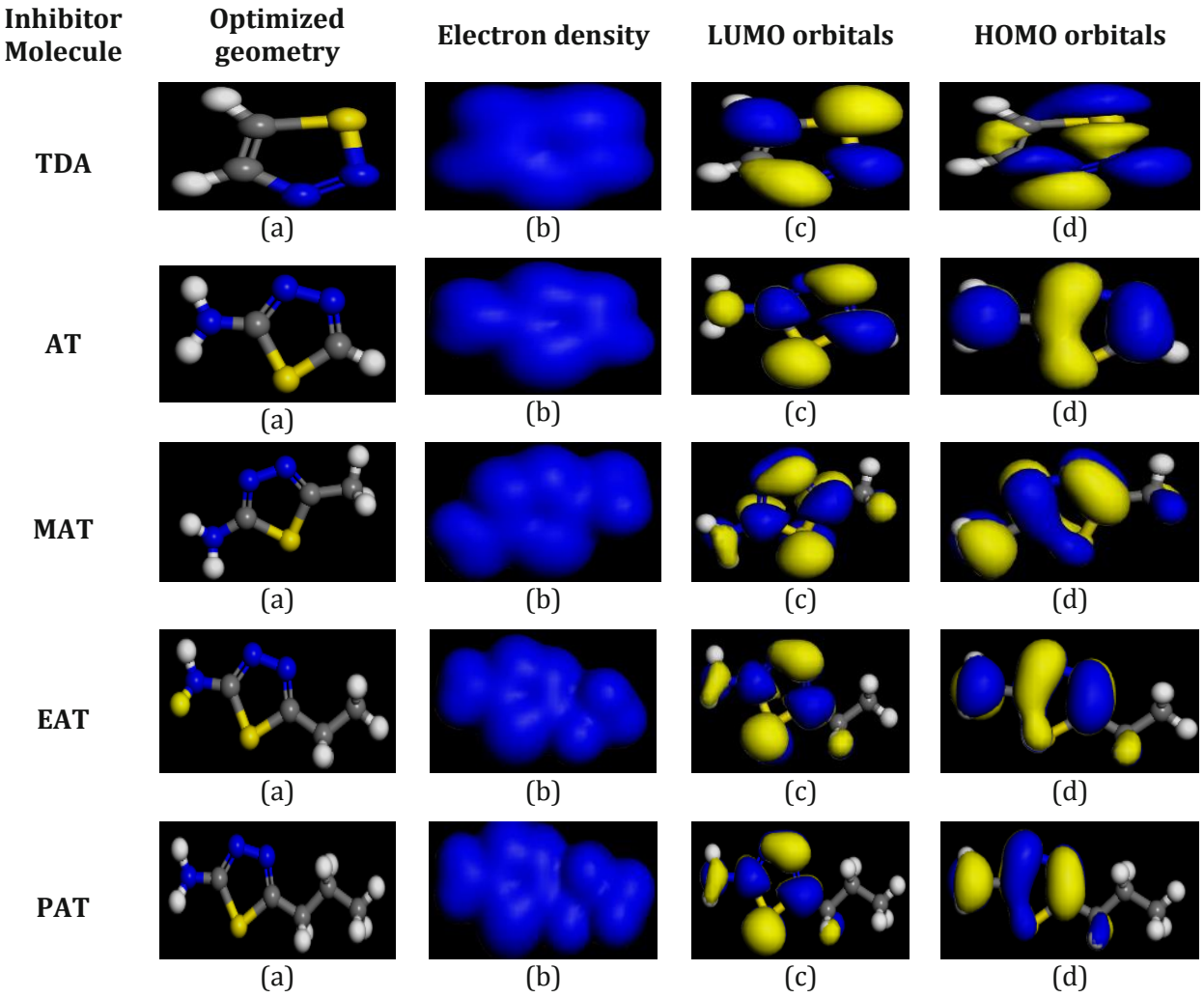

Figure 2. Structure of thiadiazole and its derivatives (a) Optimized Geometry (b) Total Electron Density (c) Highest Occupied Molecular Orbital (d) Lowest Unoccupied Molecular Orbital

Chemical Quantum Parameters

The optimized geometry, total electron density, highest occupied molecular orbital (HOMO), lowest unoccupied molecular orbital (LUMO), and other parameters of TDA, the reference molecule, were calculated and presented in Table 2. Other molecules with similar structures include 2-amino-1,3,4-thiadiazole (AT), 5-methyl-2-amino-1,3,4-thiadiazole (MAT), 5-ethyl-2-amino-1,3,4-thiadiazole (EAT) and 5-propyl-2-amino-1,3,4-thiadiazole (PAT). The optimized geometry of the studied molecules showed a nearly planar structure, which provided the optimal orientation for more significant interaction between the inhibitor molecule and the metal surface. Figure 2 also depicts the HOMO and LUMO orbitals of the compounds under study and the reference molecule. The snapshot shows that the HOMO and LUMO orbitals are dispersed throughout the entire molecule. This may be because the sulfur and nitrogen atoms have lone pair electrons, while the phenyl and thiadiazole rings have pi electrons that have been delocalized.

According to a theoretical perspective, these adsorption centers may lead to the molecules' flat orientation on the steel surface, in which case a high degree of surface coverage and inhibitory efficiency is anticipated. Figure 2 displays the

overall electron density distribution for the investigated inhibitor compounds. It is essential to remember that PAT has a higher total electron density distribution than MAT, EAT, and AT molecules, which increases the likelihood that PAT will adsorb more firmly on the iron surface than the other three thiadiazole derivatives. This explains why PAT inhibitory efficiency is higher than that of the reference molecule TDA and the other three other derivatives combined.

According to the frontier molecular orbital theory [2], a molecule's chemical reactivity depends on how it interacts and is configured with the HOMO and LUMO levels of the reacting systems. The E_{HOMO} and E_{LUMO} symbols on a molecule represent its capacity to donate electrons to a suitable acceptor with empty molecular orbitals and its capacity to accept electrons. The ability of the molecule to accept electrons increases with lower E_{LUMO} values. However, the inhibitor's ability to denote electrons to the vacant orbital of the metal surface increases with higher E_{HOMO} values, increasing the efficiency of the inhibition.

The procedure results revealed that TDA, which is anticipated to have the least corrosion inhibition among the examined compounds, has the lowest energy E_{HOMO}. The calculations revealed that the lowest value of E_{LUMO} was found in PAT and EAT molecules with the highest molecular weight and demonstrated the maximum inhibition efficiency. Lower values of E_{LUMO} denote an increase in inhibition effectiveness. On the hand, the TDA molecule, which has the highest value of E_{LUMO} shows the lowest level of inhibitory effectiveness. Additionally, it was demonstrated that the E_{LUMO} decreases as molecule molecular weight increases, which is consistent with the findings of the experimentally determined data [16-19]. Figure 2 depicts the HOMO and LUMO orbitals. Several molecular structures and conformational barriers were the subject of theoretical models developed using the HOMO-LUMO energy gap. The reference molecules, TDA and AT, have a low energy gap value, as seen in Table 2. This demonstrates that the molecule has a more significant propensity for powerful inhibitory efficiency, which rises with decreasing energy gaps and hardness values [2,4,6]. Additionally, the energy gaps between the molecules are equivalent, which may be due to similar functions.

Dipole moment is a term used to explain the interactions of inhibitor molecules in a charged environment. It was difficult to link an inhibitor molecule's dipole moment to the inhibition's efficiency [6,7,29,30]. The order of the dipole moment value in Table 2, which differs from the order indicated in the experimental results, was PAT> EAT> MAT>AT>TDA. The significant global chemical parameters were compiled in Table 2. Ionization energy is a key indicator of an atom or molecule's chemical reactivity.

High stability and chemical inertness are indicated by low ionization energy and high ionization energy, respectively [31]. PAT, EAT, and MAT has low and comparable ionization energies of 6.525 (eV), which reveal their significant inhibitory efficiency. Absolute hardness and softness are essential characteristics to gauge the stability and reactivity of molecules. It is clear that the chemical hardness, at its core, refers to the resistance to deformation or polarization of the electron cloud of the atoms, ions, or molecules under slight disruption of the chemical reaction. A soft molecule has a small energy gap compared to hard molecules with a large energy gap [32].

Other linked aspects of the molecule's electrical configuration are its ionization potential (IP) and its electron affinity (EA). The IP and EA values rise as the HOMO and LUMO values decline [33]. This demonstrates the electron movement's strong polarizability and favorable donor properties in a field. Table 2 demonstrates that the reference molecule TDA has the highest IP and EA values compared to other compounds.

Table 2. Values of structural and electronic properties of the thiadiazole and its derivatives calculated using DFT at B3LYP functional and (DNP) basis set in the aqueous phase

Properties	Inhibitors				
	TDA	AT	MAT	EAT	PAT
$E_{HOMO\ (eV)}$	-7.612	-6.485	-6.524	-6.525	-6.525
$E_{LUMO\ (eV)}$	-1.924	-0.824	-0.779	-0.770	-0.769
ΔE (eV)	5.688	5.661	5.725	5.755	5.756
Dipole moment (debye)	1.402	1.846	1.971	2.173	2.265
Molecular weight (amu)	86	101	115	129	143
Molecular area ($^0_A2$)	104.24	118.47	137.84	157.26	174.91
Molecular volume ($^0_A3$)	91.35	105.03	124.19	144.41	162.46
Ionization potential (I) (eV)	7.612	6.485	6.524	6.525	6.525
Electron affinity (A) (eV)	1.924	0.824	0.779	-0.770	-0.769
Global hardness (η)	2.844	2.831	2.873	2.878	2.878
Global softness (σ)	0.352	0.353	0.348	0.347	0.347
Absolute electronegativity (χ)	4.768	3.655	3.652	3.648	3.647
Global electrophilicity index (ω)	3.997	2.359	2.130	2.312	2.311
Nucleophilicity (ε)	0.250	0.424	0.469	0.433	0.433
Energy of back donation electron ($\Delta E_{b\text{-}d}$)	-0.711	-0.708	-0.718	-0.719	-0.719
Fraction of electron transfer (ΔN)	0.392	0.591	0.583	0.582	0.583

The interaction between the inhibitor molecule and the metal surface can also be demonstrated via the back donation $\Delta E_{b\text{-}d}$ energy. According to Nyijime *et al*. [34], the process of back donation is improved if the global hardness is positive and the energy of back donation ($\Delta E_{b\text{-}d}$) value is negative. According to Table 2, all of the molecule's global hardness values are positive, which shows that the transfer of charge from the inhibitor molecules to the iron metal occurs when the inhibitor molecules connect with the iron surface. While the electrophilicity index (ω) denotes a molecule's capacity to receive electrons. Nucleophilicity (ε), which is the inverse of electrophilicity (1/ω), refers to a molecule's propensity to donate or exchange electrons [17,28,30-35]. According to the literature, compounds with high nucleophilicity values effectively suppress corrosion, while high electrophilicity index molecules do not [27,36]. Table 2 reveals that only 3.6 electrons were transferred by the complete inhibitor molecule to the surface of the iron metal, demonstrating that the ability of these inhibitors to donate electrons to the metal surface enhanced inhibition efficiency [27,33-37]. Corrosion inhibition may be most effective for the molecule with the highest N value.

Active Sites

Table 3 displays the calculated percentage of the second-order Fukui function of the investigated inhibitor compounds, while Figure 3a–3e displays graphical depictions of the inhibitor molecules. Table 3 demonstrates that

every element in Figures 3a and 3b had a positive Fukui second function value, with no negative values for TDA and AT. On Figures 3c, 3d, and 3e of the second-order Fukui function, similar to MAT, EAT, and PAT molecules, 91.7%, 86.7%, and 88.9% of the elements all displayed positive values, while 8.3%, 13.3%, and 11.1% of the elements displayed negative values. The second-order Fukui functions of the investigated inhibitor molecules lead to the conclusion that TDA and AT are 100% nucleophilic, making them more effective at stopping the corrosion of iron metal surfaces [38].

Table 3. Calculated percentage of second-order Fukui function of the studied molecules

Inhibitor Molecule	F^{2+}%	F^{2-}%
TDA	100	0
AT	100	0
MAT	91.7	8.3
EAT	86.7	13.3
PAT	88.9	11.1

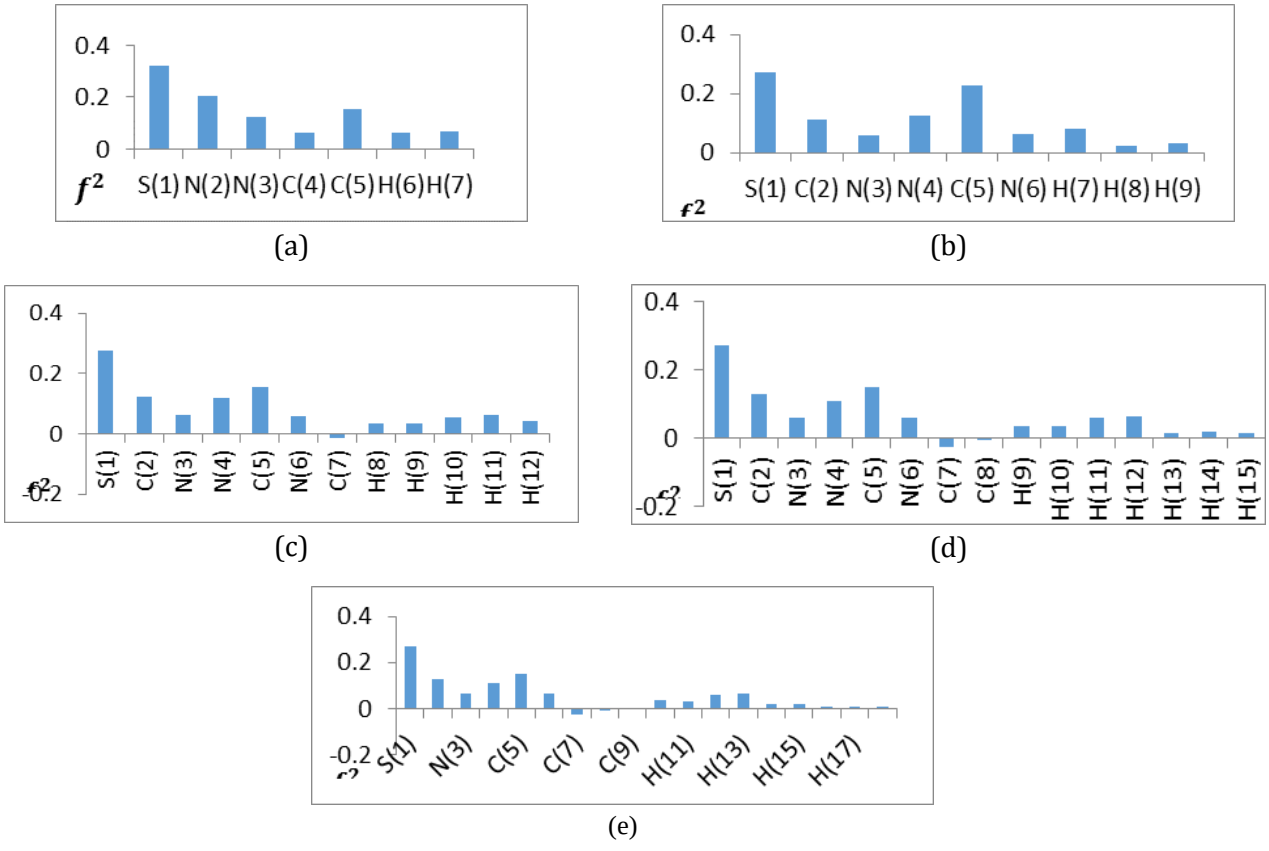

Figure 3. Graphical representation of second-order Fukui function of (a) TDA, (b) AT, (c) MAT, (d) EAT, (e) PAT

Using the Fukui indices, the active sites of the inhibitor compounds' interactions with nucleophilic (f^+) and electrophilic (f^-) assaults were studied. The nucleophilic and electrophilic attacks are controlled by the maximal f+ and f^- threshold values. The targets of a nucleophilic

assault are the atoms with the highest value of f+. Similarly, electrophilic attacks are preferred when f^- has the largest value. The examined inhibitor molecule's computed condensed Fukui functions are displayed in Table 4. Each inhibitor molecule has a higher Mulliken and Hirshfeld charge on the S(1) atom, which is the location where nucleophilic and electrophilic attacks on the molecules occur, as can be seen in Table 4.

Table 4. Fukui function parameters of the studied inhibitor molecule

		Nucleophilic attack (f^+)		Electrophilic attack (f^-)	
Compound	**Atom**	**Mulliken**	**Hirshfeld**	**Mulliken**	**Hirshfeld**
TDA	S(1)	0.323	0.325	0.253	0.252
AT	S(1)	0.271	0.269	0.189	0.170
MAT	S(1)	0.274	0.256	0.172	0.144
EAT	S(1)	0.273	0.254	0.171	0.142
PAT	S(1)	0.272	0.252	0.173	0.145

Dynamic Simulation of Molecules

Utilizing Forcite quench to sample a wide range of low-energy configurations and pinpoint the low-energy minima, molecular dynamic simulations of each inhibitor's adsorption on the metal surface were used to evaluate it at the molecular level [38,39]. The reported inhibitor molecules' adsorption on mild steel was reproduced by simulating the interactions between the inhibitor molecules and the surface of the Fe (110) crystal.

Figure 4 displays the equilibrium configurations of the simulated systems, and Table 5 contains the essential energy parameters for the systems. Figure 4 shows that the inhibitor molecules' heteroatoms and the portion of the molecule containing the aromatic rings are adsorbed on the surface of Fe (110) in a nearly flat orientation, ensuring the inhibitor molecules' best interactions with the metallic surface. An essential metric to evaluate a metal's capacity for adsorption and inhibition is the binding/adsorption energies of molecules on its surface. The stability of the inhibitor molecules adsorbed on the metal surface increases with the adsorption energy of the molecules on the metal surface. It follows that a more effective inhibitory performance is anticipated.

Table 5 shows the investigated inhibitor compounds' calculated binding/adsorption energies on the Fe (110) surface in the aqueous phase. Results reveal that, except for the reference molecule TDA, the inhibitory performance of these thiadiazole molecules rises with increasing alkyl chain length, as seen by order of the examined inhibitor molecules' binding/adsorption energy PAT>EAT>MAT>AT>TDA. This outcome shows good consistency with the experimental value reported by Quraishi and Khan [13]. Even though the simulations did not account for the unique covalent interactions between the molecules and the iron surface, the magnitudes of the calculated adsorption energies were all less than 100 kcal mol^{-1} (Table 5). According to reports, this value falls within the range of physisorption interactions [38-39]. Additionally, it has been noted that the better the inhibitor's adsorption onto the metal surface and, thus, the higher the inhibition, the more negative the adsorption energy of the inhibitor-metal contact is [40-42].

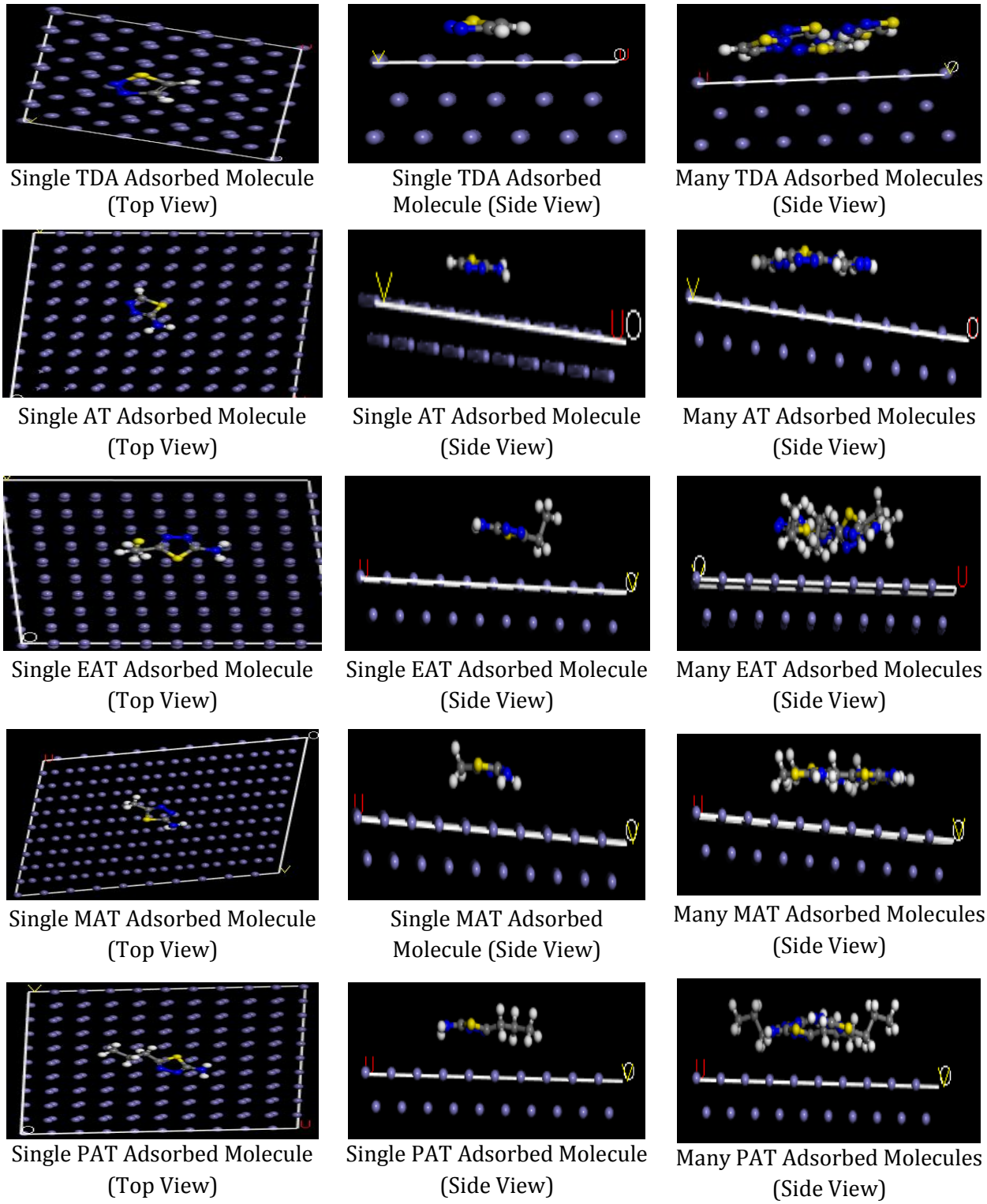

Figure 4. Snapshots of the adsorbed thiadiazole molecule on the Fe(110) surface

Table 5. Calculated molecular dynamic simulation parameters for the studied thiadiazoles

	Inhibitor molecules				
Properties (kcal.mol^{-1})	**TDA**	**AT**	**EAT**	**MAT**	**PAT**
Total kinetic energy	9.17±0.01	5.91±3.08	10.17±4.8	8.23±3.78	13.89±4.3
Total potential energy	-27.27±6.4	-60.73±0.02	-78.29±0.19	-76.03±0.004	-88.96±2.68
Energy of the molecule	-30.45±0.0	-26.01±0.01	-29.05±0.16	-33.02±0.005	-34.42±1.04
Energy of Fe(110) surface	0.00±0.00	0.00±0.00	0.00±0.00	0.00±0.00	0.00±0.00
Adsorption energy	-32.45±0.0	-34.73±0.02	-49.24±0.39	-42.99±0.005	-54.54±1.85
Binding energy	32.5	34.7	49.2	42.9	54.5

Inhibition Mechanism

Based on molecular adsorption, the inhibition of mild steel corrosion in acidic solutions by thiadiazole compounds can be explained. The molecular structures make it clear that these compounds are able to adsorb on the metal surface via the aromatic ring - electrons and the lone pair of electrons on the N and S atoms. The order of inhibitory effectiveness among the chemicals examined in the current investigation has been determined to be as follows: PAT > EAT > MAT > AT>TDA.

Conclusions

Quantum chemical calculations and molecular dynamics simulation techniques were employed to investigate the inhibitive potentials of four thiadiazole compounds on mild steel corrosion. The quantum chemical investigations of the compounds showed that PAT is more nucleophilic than AT, EAT, and MAT. The reactive sites were found on S(1) atoms and N(6) atoms using Fukui indices. This could form coordinate and back-donating bonds to enhance the absorption of thiadiazole molecules onto iron metal surfaces. Furthermore, molecular dynamics simulations showed that during the adsorption process, molecules' polar heads were adsorbed parallel to the metal surface, while their alkyl chains deviated from the metal surface at a specific inclination angle and distorted, which is consistent with earlier HOMO and LUMO orbitals analyses. It was also established from the adsorption or binding energy of the thiadiazole molecules on the Fe surface to be relatively low, signifying the physical adsorption mechanism. The reference molecule (TDA) was found to have the least inhibition efficiency in adsorption or binding energies relative to the other four derivatives, which are more promising to serve as corrosion inhibitors on the Fe surface.

Acknowledgment

The installation of the BIOVIA Material Studio 8.0 software was done with assistance from Dr. David Arthur of the Baze University in Abuja, Nigeria, which the authors gratefully welcome.

Disclosure statement

The authors declare that they have no conflict of interest.

Orcid

Thomas A. Nyijime: 0000-0001-9537-1987
Habibat F. Chahul: 0000-0002-0504-231x
Abdullahi M. Ayuba: 0000-0002-2295-8282
Fater Iorhuna: 0000-0002-1018-198x

References

[1] A.S. Fouda, A.A. Ibrahim, W.T. El-behairy, *Der Pharma Chemica*, **2014**, 6, 144–157. [Google Scholar]

[2] T.A. Nyijime and I. Iorhuna, *Appl. J. Envir. Eng. Sci*. **2022**, 8, 237–249. [Crossref], [Google Scholar], [Publisher]

[3] K. Sadik, S. Bayadi, M.E. Hachim, N. El-Hamdani, C. Podlipnik, A. Aboulmouhajir, Journal of molecular structure, **2021,** *1240*, 130571. [CrossRef], [Google Scholar], [Publisher]

[4] C. Verma, M.A. Quraishi, E.E. Ebenso, *Sustain. Chem. Pharm*., **2018**, *10*, 134–147. [CrossRef], [Google Scholar], [Publisher]

[5] I.B. Obot, N.O. Obi-egbedi, S.A. Umoren, *Corros. Sci*., **2009**, *51*, 1868–1875. [CrossRef], [Google Scholar], [Publisher]

[6] Y. Boughoues, M. Benamira, L. Messaadia, N. Bouider, S. Abdelaziz, *RSC Adv*., **2020**, *10*, 24145–24158. [CrossRef], [Google Scholar], [Publisher]

[7] X. Luo, C. Ci, J. Li, K. Lin, S. Du, H. Zhang, X. Li, Y.F. Cheng, J. Zang, Y. Liu, *Corrosion Sci.*, **2019**, 151, 132–142. [CrossRef], [Google Scholar], [Publisher]

[8] N.O. Obi-Egbedi, I.B. Obot, M.I. El-Khaiary, S.A. Umoren, E.E. Ebenso, *Int. J. Electrochem. Sci.,* **2011**, 6, 5649–5675. [Google Scholar]

[9] U. Umar, A.M. Ayuba, *RHAZES: Green Appl. Chem*., **2020**, 10, 113–128. [Google Scholar], [Publisher]

[10] H. Lgaz, S. Masroor, M. Chafiq, M. Damej, A. Brahmia, R. Salghi, M. Benmessaoud, I.H. Ali, M.M. Alghamdi, A. Chaouiki, I.M. Chung, *Metals*, **2020**, 10, 357. [CrossRef], [Google Scholar], [Publisher]

[11] H. Zhang, Y. Chen, Z. Zhang, *Result Phys*. **2018**, 11, 554–563. [CrossRef], [Google Scholar], [Publisher]

[12] M. Talari, S.M. Nezhad, S.J. Alavi, M. Mohtashamipour, A. Davoodi, S. Hosseinpour, *J. Mol. Liq*., **2019**, *286*, 110915. [CrossRef], [Google Scholar], [Publisher]

[13] S.S. Khemalapure, V.S. Katti, C.S. Hiremath, S.M. Hiremath, M. Basanagouda, S.B. Radder, *J. Mol. Struct*., **2019**, *1196*, 280–290. [CrossRef], [Google Scholar], [Publisher]

[14] D. Alokdut, K.S. Sourav, A. Utpal, B. Priyabrata, S. Dipankar, *Corros Sci,* **2017**, 123, 256–266. [Google Scholar]

[15] N.O. Eddy, P.O. Ameh, O.O. Anduang, E.E. Ebenso, *Int. J. Electrochem. Sc.i,* **2011**, 7, 7425–7439. [Google Scholar]

[16] K.S. Sudhish, E.E. Eno, *Int. J. Electrochem. Sci.*, **2011**, 6, 3277-3291. [Google Scholar]

[17] J. Lou, H. Wang, S. Wang, J. Han, M. wang, Journal of molecular structure, **2022,** 1267, 133629. [CrossRef], [Google Scholar], [Publisher]

[18] R.D. salim, Q.A. Jawad, K.S. Ridah, L.M. Shakar, A.A. Al-Amirey, A.A. Kadhum, M.S. Takriff, int. J. Corros. Scale inhib. **2020,** 9, 550–561. [CrossRef], [Google Scholar]

[19] M.A. Quraishi & S. Khan, *Indian Journal of Chemical Technology,* **2005**, 12, 576–581. [Google Scholar]

[20] K.M. Zohdy, R.M. El-Sherif, S. Ramkumar,A.M. El-Shamy, *Upstream Oil Gas Technol.,* **2021**, 6, 100025. [CrossRef], [Google Scholar], [Publisher]

[21] Y. Boughoues, M. Benamira, L. Messaadia, N. Bouider, S. Abdelaziz, *RSC Adv*., **2020**, *10*, 24145–24158. [CrossRef], [Google Scholar], [Publisher]

[22] F. Iorhuna, A.S. Muhammad, M.A. Ayuba, *Adv. J. Chem. A*, **2023,** *6*, 71–84. [CrossRef], [Publisher]

[23] V.H. Rezvan, *Adv. J. Chem. A*, **2022,** 5, 10–21. [CrossRef], [Google Scholar], [Publisher]

[24] V.S. Sastri and J.R. Perumareddi, *Corrosion,* **1997**, *53*. [Google Scholar], [Publisher]

[25] T. Koopmans, *Physica*, **1993**, 1, 104–113. [CrossRef], [Google Scholar], [Publisher]

[26] F.E. Awe, S.O. Idris, M. Abdulwahab, E.E. Oguzie, *Cogent-Chemistry* **2015**, 1, 1112676. [CrossRef], [Google Scholar], [Publisher]

[27] O.M. Akinlosotu, B.T. Ogunyemi, B.B. Adeleke, Advanced journal of chemistry-section A, **2022,** 5, 70–80. [CrossRef], [Google Scholar], [Publisher]

[28] G. Bereket, E. Hur,C. Ogretir, *J. Mol. Struct. (Theochem),* **2002**, *578*, 79–88. [CrossRef], [Google Scholar], [Publisher]

[29] A. Hamil, K.M. Khalifa, A.A. Almutaleb, M.Q. Nouradean, *Adv. J. Chem. A*, **2020**, *3*, 524–535. [CrossRef], [Google Scholar], [Publisher]

[30] N.D. Ojo, R.W. Krause, N.O. Obi-Egbedi. *J. Mol. Liq*., **2020**, *319*, 1–8. [CrossRef], [Google Scholar], [Publisher]

[31] L. Guo, M. Zhu, J. Chang, R. Thomas, R. Zhang, P. Wang, *Int. J. Electrochm. Sci.,* **2021,** 16, 211139. [Google Scholar],

[32] A. Behmanseh, F. Salimi, G.E. Rajaei. *Monatsh. Chem*., **2020**, *151*, 25–32. [CrossRef], [Google Scholar], [Publisher]

[33] O.A. Odewole, C.U. Ibeji, H.O. Oluwasola, O.E. Oyeneyin, K.G. Akpomie, C.M. Ugwu, C.G. Ugwu, T.E. Bakare, *J. Mol. Struct.,* **2021**, *1223*, 129214. [CrossRef], [Google Scholar], [Publisher]

[34] T.A. Nyijime, A.M. Ayuba and H. F. Chahul, *J. New Technol. Mater.,* **2022**, 12, 80–88.

[35] F.E. Ani, C.U. Ibeji, N.L. Obasi, M.T. Kelani, K. Ukogu, G.F. Tolufashe, S.A. Ogundare, O.E. Oyeneyin, G.E.M. Maguire, H.G. Kruger, *Sci. Rep*., **2021**, *11*, 8151. [Google Scholar]

[36] K. Rasheeda, D. P. Vijaya, P. A. Alva, Krishnaprasad, S. Samshuddin, *Int. J. Corros. Scale Inhib*, **2018**, 7, 48–61. [CrossRef], [Google Scholar], [Publisher]

[37] S.P. Yeddu, P. Thangaiyan, A. Veeraiah, D. Vijay, K.E. Srikanth, A. Irfan, R. Thomas, *Biointerface Res. Appl. Chem*., **2022**, *12*, 3996–4017. [CrossRef], [Google Scholar]

[38] T.A. Nyijime, A.M. Ayuba, H.F. Chahul, *Bull Natl Res Cent* **2021**, *45*, 189. [CrossRef], [Google Scholar], [Publisher]

[39] T.A. Nyijime, A.M. Ayuba, *Appl. J. Envir. Eng. Sci*., **2020**, 6, 344–355. [CrossRef], [Google Scholar], [Publisher]

[40] I.B. Obot, K. Haruna, T.A. Saleh, *Arabian J. Sci. & Eng*., **2018**. [CrossRef], [Google Scholar], [Publisher]

[41] A.M. Ayuba, A. Uzairu, H. Abba, G.A. Shallangwa, *Morrocan Journal of Chemistry*,vol. 6, **2018,** 6, 160–172.

[42] B.T. Ogunyemi, D.F. Latona, A.A. Ayinde, I.A. Adejoro, *Adv. J. Chem. A,* **2020**, *3*, 485–492. [CrossRef], [Google Scholar], [Publisher]

HOW TO CITE THIS ARTICLE

Thomas Aondofa Nyijime *, Habibat Faith Chahul, Abdullahi Muhammad Ayuba, Fater Iorhuna. Theoretical Investigations on Thiadiazole Derivatives as Corrosion Inhibitors on Mild Steel. *Adv. J. Chem. A*, **2023**, 6(2), 141-154.

DOI: 10.22034/AJCA.2023.383496.1352
URL: http://www.ajchem-a.com/article_168060.html